Applied Catalysis B: Environmental 341 (2024) 123317

Contents lists available at ScienceDirect

Applied Catalysis B: Environmental

journal homepage: www.elsevier.com/locate/apcatb

The mega-merger strategy: M@COF core-shell hybrid materials for facilitating CO_2 capture and conversion to monocyclic and polycyclic carbonates

Ping Liu [a,b], Kaixing Cai [a,b], Duan-Jian Tao [c], Tianxiang Zhao [a,b,*]

[a] Key Laboratory of Green Chemical and Clean Energy Technology, School of Chemistry and Chemical Engineering, Guizhou University, Guiyang 550025, PR China
[b] Engineering Research Center of Efficient Utilization for Industrial Waste, Guizhou University, Guiyang, Guizhou 550025, China
[c] College of Chemistry and Chemical Engineering, Jiangxi Normal University, Nanchang 330022, PR China

ARTICLE INFO

Keywords:
CO_2
Metal-organic frameworks
Covalent organic frameworks
M@COF hybrid materials
Cyclic carbonate

ABSTRACT

Metal-organic frameworks (MOFs) and covalent organic frameworks (COFs) have garnered significant attention for their potential in CO_2 capture and conversion, owing to their unique properties. However, these materials suffer from inherent drawbacks such as poor stability and catalytic activity, leading to unsatisfactory utilization efficiency. In this work, we fabricated a series of novel M@COF hybrid materials by growing pyridine-based COFs with varying thicknesses on NH_2-UiO-66 cores. These materials exhibited large specific surface areas and favorable chemical stability. The combination of the high specific surface area of MOF and the multiple interacting π-π stacking interactions of COF in these M@COF hybrid materials resulted in significantly enhanced CO_2 adsorption performance, surpassing that of individual parent MOF or COF. In addition, an ion-functionalized M@COF-0.15-Br was fabricated through a simple post-synthesis modification. The presence of abundant ion active sites and interfacial synergistic effects in M@COF-0.15-Br effectively facilitated activation of reactants, enabling efficient catalytic conversion of CO_2 to monocyclic and polycyclic carbonates. Consequently, the superior CO_2 capture and conversion achieved using this M@COF core-shell hybrid material offers a new approach to design advanced functional materials with optimized structures for CO_2 capture and conversion.

1. Introduction

Metal organic frameworks (MOFs), composed of metal ions (or metal clusters) and organic ligands assembled through coordination bonds, belong to a burgeoning category of porous crystalline materials with uniform pore sizes and large surface areas, are widely used in the fields of adsorption and catalysis [1,2]. However, the coordination bond connecting of MOFs is exceptionally unstable, resulting in limitations across their performance spectrum [3]. Covalent organic frameworks (COFs) represent another prominent class of crystalline porous organic polymers. Unlike MOFs, COFs are bonded by strong covalent bonds but offer similar properties [4,5]. Notably, COFs have garnered significant attention due to their remarkable physicochemical stability and ease of structural modification [6]. However, COFs typically consist of only light weight elements such as carbon (C), nitrogen (N), and oxygen (O), which undermines their catalytic activity. Consequently, most catalytic systems involving COFs necessitate the inclusion of co-catalysts for optimal performance [7]. Additionally, achieving controlled synthesis of COFs poses a formidable challenge. To leverage the strengths of both MOFs and COFs, the amalgamation of the two has emerged as the favored approach, that is, a strategy known as the "mega-merger strategy" [8].

Cooperation between MOFs and COFs enables the integration of prepared MOFs into the synthesis of COFs, resulting in the formation of M@COFs core-shell hybrid structure [9–11]. This core-shell structure exhibits exceptional synergistic properties as M@COFs inherit the advantages of high surface area, uniform pore size, stable physicochemical properties, and facile structural modification inherited from the parent MOFs or COFs [12,13]. Moreover, the covalent bonding between N-containing and O-containing organic groups in COFs grafted onto MOFs significantly enhances the adsorption capacity of the hybrid materials [14,15]. Additionally, the structural synergistic effect at the

* Corresponding author at: Key Laboratory of Green Chemical and Clean Energy Technology, School of Chemistry and Chemical Engineering, Guizhou University, Guiyang 550025, PR China.
E-mail address: chemcaicai@yeah.net (T. Zhao).

https://doi.org/10.1016/j.apcatb.2023.123317
Received 15 August 2023; Received in revised form 14 September 2023; Accepted 18 September 2023
Available online 20 September 2023

core-shell interface effectively facilitates the charge transfer between the two components, thereby addressing the issue of insufficient catalytic activity in the two-component catalytic system [13,16].

The controlled synthesis of M@COFs has garnered significant attention in recent years due to the influential role that M@COFs hybrid materials play in catalysis, adsorption, and sensors [14,17]. For instance, Li et al. [18] constructed a series of composites by using NH_2-MIL-101 (Fe) as the core and growing NUT-COF-1 (NTU) in-situ on the MOF core as the shell layer. These composites displayed outstanding catalytic conversion and selectivity in styrene oxidation. Similarly, Wang et al. [19] developed MIL-125 @TAPB-PDA nanomaterials as stable photocatalysts for efficient catalytic photo-oxidation of aromatic alcohols. In terms of separation, Wang et al. [20] prepared an NH_2-UiO-66 @Br-COFs hybrid material prepared that exhibited remarkable performance in both CO_2 and I_2 vapor trapping due to the synergistic effect between the core and shell. Additionally, Zhao et al. [21] demonstrated that M@COFs can be employed as a hybrid matrix membrane seasoning for achieving highly selective capture of CO_2. These results collectively showcase the superior performance of M@COFs compared to their parent materials, thereby fostering further comprehensive research in this field. Despite considerable advancements, the existence of M@COFs hybrid materials with combined CO_2 adsorption and catalytic conversion properties remains scarce.

Herein, we designed a pyridine-based COF for in situ growth on a MOF core, NH_2-UiO-66. By varying the thickness of the pyridine-based COF shell layer, a series of M@COFs hybrid materials were prepared. Compared to the parent COF and MOF, these M@COFs hybrid materials exhibited significant advantages, including higher physicochemical stability and stronger π-π stacking interactions, resulted in a significant increase in their CO_2 adsorption capacity. To further enhance the functionality of the M@COFs, an ion functionalized hybrid material, M@COF-0.15-Br, with active side chains was also fabricated by a simple post-synthesis modification (PSM) strategy, eliminating the need for external catalyst, additional reagents, or harsh reaction conditions for the cycloaddition of CO_2 and epoxides [22]. As a proof of concept, we successfully obtained both monocyclic and polycyclic carbonates in excellent yields.

2. Experimental

2.1. Materials

1,3,5-tris(4-formylphenyl)benzene (TFB, ≥95%), 2,6-diaminopyridine (Diam, ≥98%), 2-aminoterephthalic acid (NH_2-BDC, ≥98%), zirconium chloride ($ZrCl_4$, ≥99%), 1-butanol (*n*-BuOH, ≥99%), 1,3,5-trimethylbenzene (≥99.5%), acetic acid (≥99.5%), and 2-bromoethanol (≥99.5%) were purchased from Energy Chemistry, Anhui Zesheng Technology Co., Ltd. All solvent and epoxides used in the experiment were purchased from Adamas Reagent without purification.

2.2. Characterizations

The physicochemical properties of the materials were characterized by scanning electron microscopy (SEM, Quanta FEG 650) and scanning transmission electron microscopy (TEM, FEI G2 F20). The crystal structure of the material was measured by an X-ray diffraction (XRD) (D8 advanced) instrument. The ^{13}C MAS NMR of the hybrid materials was characterized by a Bruker 400 M. X-ray photoelectron spectroscopy (XPS) (K-Alpha Plus) was used to determine the surface elemental composition of the hybrid materials. The thermal stability of the material was measured by thermogravimetric analysis (TGA) (TG 209F1Libra). Fourier transform infrared (FTIR) spectra and in situ FTIR spectra were measured by Nicolet 50 FTIR advanced spectroscopy. N_2 adsorption-desorption curves and CO_2 adsorption curves were tested by a BSD-PM2 instrument. The yield of cyclic carbonates was determined using a Shimadzu GC-2014 gas chromatograph in conjunction with ^1H NMR.

2.3. Synthesis of materials

2.3.1. Synthesis of NH_2-UiO-66

To prepare the NH_2-UiO-66, 208 mg of $ZrCl_4$ and 163 mg of NH_2-BDC were separately dissolved in 35 mL of DMF. The solutions were then stirred to form clear solutions, after which 12 mL of acetic acid was added. The resulting mixed solution was transferred to a 100 mL Teflon-lined stainless-steel autoclave and heated at 120 °C for 12 h. After the reaction, the product NH_2-UiO-66 was collected through filtration, washed with DMF and methanol, and finally dried under vacuum overnight at 80 °C.

2.3.2. Synthesis of COF

The pyridine-based COF was synthesized according to the method described by Cui et al. [23]. In brief, 0.15 mmol of TFB and 0.23 mmol of Diam were dissolved in a mixed solution of 2.0 mL of *n*-BuOH and 1 mL of 1,3,5-trimethylbenzene. The mixture was sonicated for 30 min until fully dissolved, after which 0.2 mL of 9 $mol \cdot L^{-1}$ acetic acid was added. The resulting solution was then frozen rapidly using a liquid N_2 bath, evacuated several times, and sealed in a Schlenk tube. The Schlenk tube was allowed to reach room temperature and then heated at 120 °C for 3 days. The resulting yellow solid, namely pyridine-based COF, was separated by centrifugation, washed with THF, methanol, and acetone, and subsequently dried under vacuum at 60 °C.

2.3.3. Synthesis of M@COF hybrid materials

Preparation of a series of M@COF hybrid materials was conducted using a one-pot method (Scheme 1) [13]. In a typical procedure for synthesis of M@COF-0.15, a solution containing 50 mg of NH_2-UiO-66 and 0.15 mmol of TFB was prepared, followed by the addition of 0.23 mmol of Diam after 30 min of sonication. Additionally, 0.2 mL of acetic acid was added during continued sonication. The resulting solution was rapidly frozen and sealed in a liquid N_2 bath. The remaining steps of the synthesis followed the same procedure as COF synthesis. Furthermore, the effect of different shell thicknesses was investigated by varying the ratio of TFB and Diam. M@COF-0.05 and M@COF-0.1 were prepared in accordance with a similar synthesis method.

To evaluate the catalytic properties of the hybridized materials, the pre-synthesized M@COF-0.15-Br shell layers were modified post-synthesis using bromoethanol. This involved slowly adding 0.5 mmol of bromoethanol dropwise to an acetonitrile solution that contains 100 mg of M@COF-0.15-Br, followed by stirring for 24 h at 80 °C and subsequent centrifugation to collect the functionalized M@COF-0.15-Br materials with active side chains. Using a similar method, ion functionalized COF-Br was also prepared.

2.4. CO_2 adsorption

The isothermal adsorption profiles of CO_2 and N_2 were measured on a BSD-PM2 specific surface area and microporous analyzer. Before testing, the adsorbent was degassed at 120 °C for 8 h to eliminate any gaseous impurities from the sample pores. Subsequently, the adsorbent was cooled down and loaded into the test system for measurement. To assess the cycling performance CO_2, the adsorbed saturated was re-degassing and subjected to 10 continuous cycles.

2.5. CO_2 conversion

A specific quantity of catalyst and 10 mmol of allyl glycidyl ether (AGE) were introduced into a 50 mL stainless steel autoclave. Prior to the reaction, the reactor was purged with CO_2 and subsequently injected with 1.0 MPa of CO_2. The reaction proceeded at a temperature of 120 °C for a duration of 12 h. The resulting mixture was assessed by GC in order to determine the yield of cyclic carbonate. To recover the catalyst

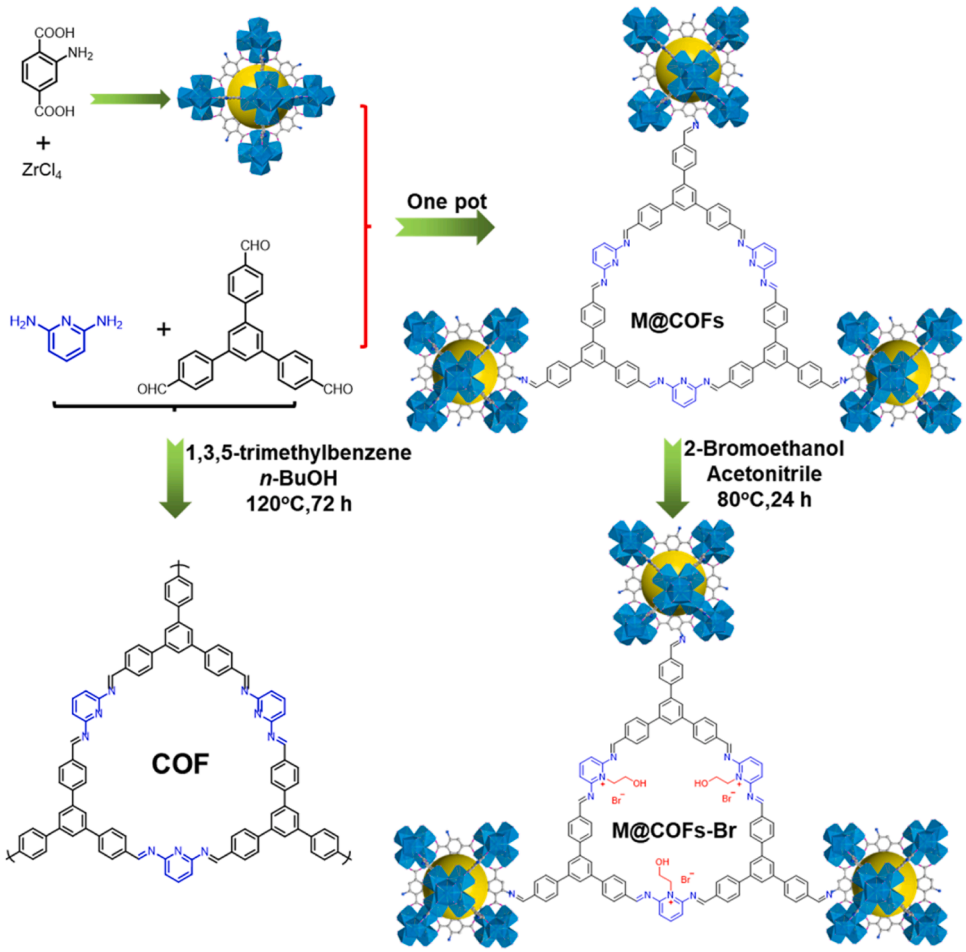

Scheme 1. The synthetic pathway for M@COF hybrid materials.

M@COF-0.15-Br, about 10 mL of ethyl acetate was added to the reaction mixture once the reaction was finished. After that, the catalyst was separated by centrifugation, washed with ethyl acetate three times (3 × 2 mL), subsequently utilized in the next catalytic cycle. The stability and structural changes of the recovered catalyst were assessed through FTIR, XRD, and TGA analysis.

3. Results and discussion

3.1. Characterization of materials

M@COF hybrid materials with varying shell layer thicknesses were prepared by adjusting the concentration of synthetic COF precursors. Initially, a fixed amount of NH_2-UiO-66 (50 mg) was chosen as the growth core, and M@COF hybrid materials with different shell layer thicknesses were fabricated by controlling the COF concentration. These M@COF hybrid materials were named as M@COF-0.05, M@COF-0.1, and M@COF-0.15, with the COF layer thicknesses ranging from thin to thick while maintaining a constant molar ratio of TFB/Diam at 3:2. The surface morphology of the hybrid material was characterized by SEM images. As depicted in Fig. 1a, NH_2-UiO-66 exhibited a uniform regular octahedral structure with an exceptionally surface. In contrast, COF exhibited a rough and uniform spherical shape (Fig. 1b). Interestingly, the surface of NH_2-UiO-66 gradually became rougher as the COF shell layer grew. Additionally, the surface of the hybrid material transformed from a rough octahedral in M@COF-0.05 to a spherical shape as the shell layer thickness increased (Fig. 1c-e), eventually becoming completely covered by the COF shell layer. These results were further validated by TEM images. Fig. 1g and h illustrate the uniform growth of COF on the surface of NH_2-UiO-66. Additionally, as the proportion of COFs increase, the thickness of the COF shell layer encapsulating the NH_2-UiO-66 surface increases from 60 nm to 138 nm. Notably, a well-defined core-shell interface is formed between MOF and COF, with both materials containing abundant pore channels. Collectively, these findings provide strong evidence that the M@COF hybrid materials featuring core-shell heterogeneous frameworks were successfully prepared.

Similarly, the morphology of M@COF-0.15 remained highly consistent before and after bromine functionalization, suggesting that the PSM strategy employed did not disrupt the structure integrity of the material itself. Furthermore, energy dispersive spectroscopy (EDS) mapping revealed that C, N, O, Zr, and Br elements were uniformly dispersed throughout the M@COF-0.15-Br hybrid material. Notably, the dispersion of Br elements appeared in a core-shell structure, while the dispersion of the Zr element was shrinked due to their encapsulation within COF. These results further support the successful synthesis of the core-shell hybrid materials.

Unlike the physical doping approach, the M@COF hybrid material is produced through a condensation reaction between an amino group (-NH_2) from the MOF core and an aldehyde group (-CHO). This reaction forms an imine bond (-C═N-), leading to a stronger connection between the MOF and COF [24,25]. This conclusion is supported by the results shown in Fig. S1a. The disappearance of the -NH_2 peak at 1658 cm^{-1} indicates that the -NH_2 on NH_2-UiO-66 reacted with the added aldehyde linker (TFB). Furthermore, the presences of the imine bond (-C═N stretching) signal at 1622 cm^{-1} affirms the completion of the condensation reaction [14,26]. Similarly, the formation of the imine bond-linked COF is further confirmed by FTIR analysis in Fig. 2a. The peaks near 3400 cm^{-1} in NH_2-UiO-66 correspond to the asymmetric

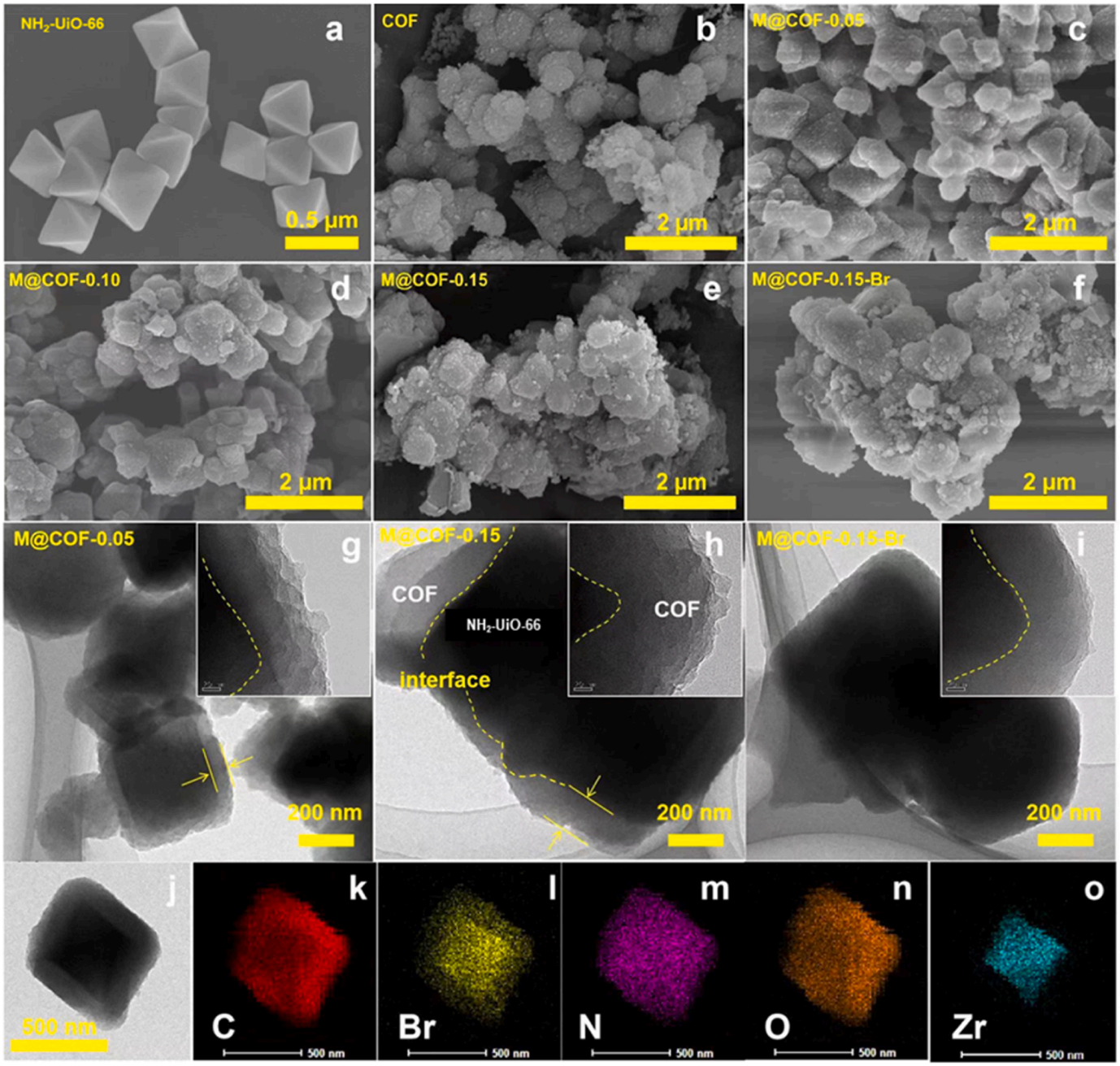

Fig. 1. SEM images of (a) NH_2-UiO-66; (b) COF; (c-e) M@COFs; (f) M@COF-0.15-Br; (g-i) TEM images of M@COFs; (j-o) elemental mapping images of M@COF-0.15-Br.

telescoping vibration of the primary amine (-NH_2) [27]. This vibration provides numerous active sites for the growth of the COF shell layer. As the shell thickness increases, the signal at this site significantly weak, indicating that a large amount of -NH_2 reacts with the aldehyde group in M@COF [28]. Additionally, characteristic peaks at 1576 cm^{-1} and 1384 cm^{-1} correspond to the symmetric and asymmetric stretching vibrations of C═O in NH_2-UiO-66, while the peak at 662 cm^{-1} belongs to the Zr-O stretching vibration [11]. Furthermore, the peak at 1211 cm^{-1} is attributed to the C-N stretching vibration in the COF [21]. For M@COF-0.15 after bromination, there was no significant change except for a new peak at 3168 cm^{-1} (-OH). These results suggest that the condensation of -NH_2 and -CHO plays a key role in the formation of the core-shell structure.

The crystal structure of M@COF was investigated using XRD (Fig. 2b and S1). As shown in Fig. S1b, the COF material exhibits a strong and sharp characteristic peak at $2\theta = 2.4°$, indicating a high crystallinity. This peak can be associated with the diffraction signal from the (100) crystal plane of COF material [29–31]. At the same time, the peak at $2\theta = 21.5°$ can correspond to the (001) crystal plane [32,33]. In contrast, the characteristic diffraction peaks of both NH_2-UiO-66 and COF were observed in M@COF. This indicates that the NH_2-UiO-66 core remained intact in the M@COF material, while the COFs shell layer successfully coated the core. The ^{13}C CP-MAS NMR spectrum further confirms this conclusion. In Fig. 2c, M@COF-0.15 exhibits the characteristic peak of NH_2-UiO-66 at 171 ppm [13,34], as well as the characteristic peak of the C═N bond of COF at 157 ppm [33,35,36]. This suggests that the hybrid material combines the characteristics of NH_2-UiO-66 and COF.

The permanent porosity of the synthesized samples was evaluated through N_2 adsorption and desorption experiments conducted at 77 K.

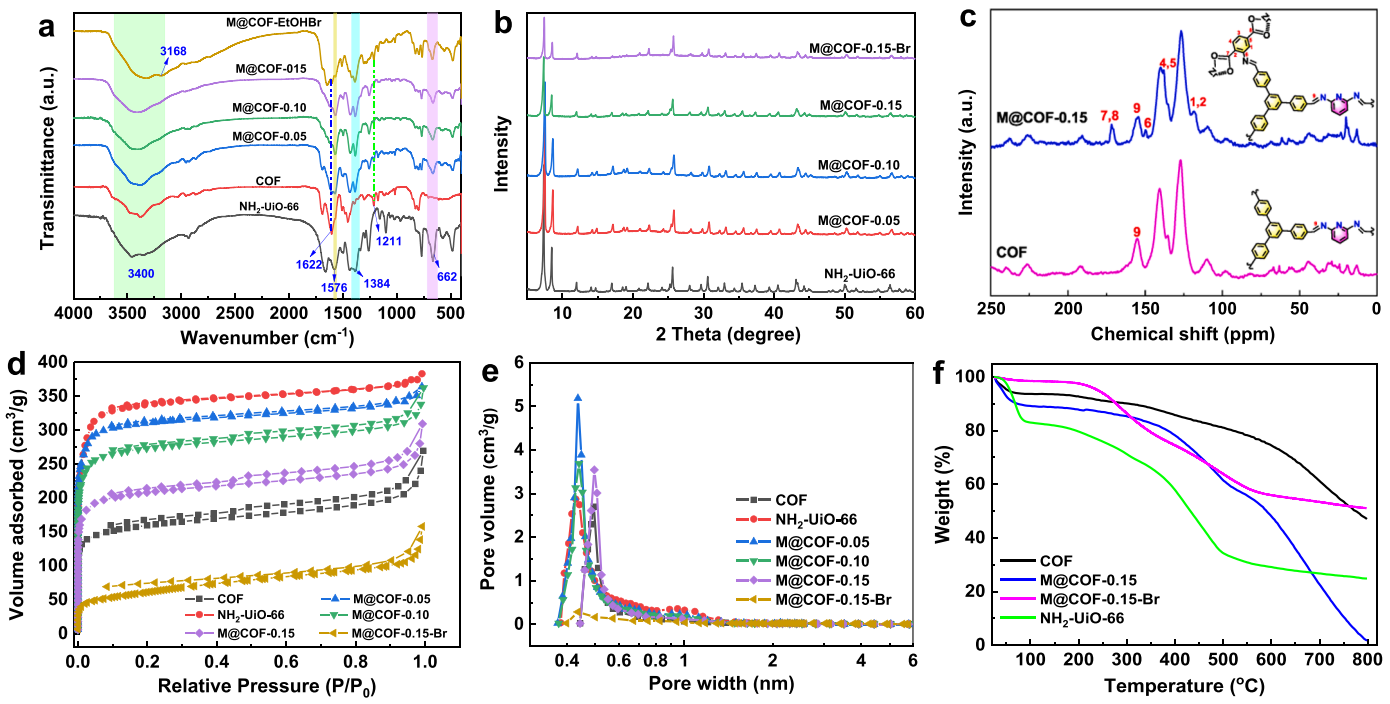

Fig. 2. (a) FTIR spectra; (b) XRD patterns; (c) ^{13}C CP-MAS NMR spectra; (d) the N_2 adsorption-desorption isotherms; (e) pore size distribution; and (f) TGA curve of NH_2-UiO-66, COF, and M@COF hybrid materials.

The pure COF and NH_2-UiO-66 exhibited a significant number of microporous voids, with BET surface areas of 498 $m^2 \cdot g^{-1}$ and 1041 $m^2 \cdot g^{-1}$, respectively. The BET surface areas of the M@COF hybrid materials are in the middle of the range (Fig. 2d). Furthermore, the pore size of the M@COF hybrid materials decreased as the thickness of the shell layer decreased (Fig. 2e). In addition, the BET surface area of the bromine functionalized M@COF-0.15-Br was significantly reduced due to the infiltration of bromine ethanol into its pores. The thermal stability of materials was also tested (Fig. 2f), TGA curves show that both the COF and M@COF materials exhibit high thermal stability below 400 °C.

The electronic state and chemical composition of the prepared materials were analyzed by XPS (Fig. 3). The high-resolution C 1 s spectrum of M@COF-0.15 can be divided into three peaks: C═C/C-C, C═N/C-N, and C-O. The peaks C═C/C-C and C═N/C-N correspond to the COF shell (C═N arises from the formed imine covalent bond), while C-O is assigned to the NH_2-UiO-66 core [20,37]. Additionally, the high-resolution N 1 s spectrum of NH_2-UiO-66 displays only one peak at 399.7 eV for C-N (Fig. 3b), whereas the N 1 s spectrum of COF exhibits two peaks at 399.1 eV for C-N and 400.3 eV for C═N [9,38]. Interestingly, the N 1 s spectrum of M@COF-0.15 shows similar features to that of COF, providing sufficient evidence for the growth of a COF shell layer on the MOF. Moreover, Fig. S2 presents the XPS spectra of M@COF-0.15-Br with active side chains. In contrast to M@COF-0.15, the N 1 s spectrum exhibits a new peak at 401.4 eV, which suggests the formation of quaternary amine nitrogen after bromine functionalization [39,40]. For M@COF-0.15-Br, the binding energy peaks of bromine ion (Fig. S2d) appear at 69.2 eV for the Br $3d_{3/2}$ and 67.9 eV for the $3d_{5/2}$ levels [41], respectively, confirming the successful branching of bromoethanol-active side chains to M@COF-0.15-Br, as achieved through the PSM strategy.

3.2. CO_2 adsorption

The CO_2 adsorption capacity at 273 K was determined using a gas adsorption instrument and a volumetric method. As depicted in Fig. 4a, NH_2-UiO-66 and COF exhibited CO_2 uptake of 3.25 mmol·g^{-1} and 2.23 mmol·g^{-1} at 1 bar, respectively. Significantly, the M@COF hybrid materials displayed a higher CO_2 adsorption capacity, with M@COF-0.05 reaching 4.53 mmol·g^{-1} at same conditions. To investigate the reasons for this increase in adsorption, we examined the BET surface area, pore volume, and CO_2 adsorption of these materials (Fig. 4b). The result indicated that materials with higher BET surface area and pore volume had higher CO_2 adsorption capacities. However, despite having a high BET surface area and pore volume, NH_2-UiO-66 exhibited lower CO_2 adsorption than that of the M@COF hybrid materials. This suggests that the limited number of active sites in NH_2-UiO-66 restricts its CO_2 uptake [42]. For M@COF hybrid materials, the higher CO_2 adsorption can be attributed to the following factors: (i) the excellent pore structure of M@COF materials and the presence of multiple active sites facilitate physical adsorption of CO_2, while the exposed Zr metal cluster further enhances adsorption by weak chemical interactions with CO_2 [43]; (ii) increased π-π stacking interactions and the presence of different N heterocycles in the M@COF skeleton promote CO_2 adsorption compared to pure NH_2-UiO-66 (the presence of N element in the COF shell enhances the basicity and surface polarity, thereby strengthening the interaction between CO_2 and the adsorbent) [44,45].

We compared the CO_2 adsorption performance of M@COF hybrid materials with several adsorbents reported in the literature by examining their adsorption performance at 273 K and 1 bar (Table 1). The CO_2 adsorption performance and adsorption selectivity of as-prepared M@COF hybrid materials surpass those of most MOF or COF adsorbents. However, it should be noted that although MOF-74(Ni)– 24–140 and HKUST-1/ANF-72 demonstrate higher CO_2 adsorption performance, they exhibit lower absorption selectivity and poor hydrothermal stability, making them unsuitable for practical application.

The adsorption behavior of the COF and M@COF materials was further investigated using Langmuir and Freundlich isotherm models, respectively (adsorption isotherm model description see supporting information). The fitting results are shown in Fig. 4c-f and Tables S1 and 2. The results indicate that the adsorption isotherms of multiple adsorbents are in excellent agreement with the Freundlich model. The R^2 value based on this model is greater than 0.995, and the value of q_e representing CO_2 adsorption closely matches the actual adsorption value. Additionally, the $1/n$ value in the Freundlich model for all adsorbents

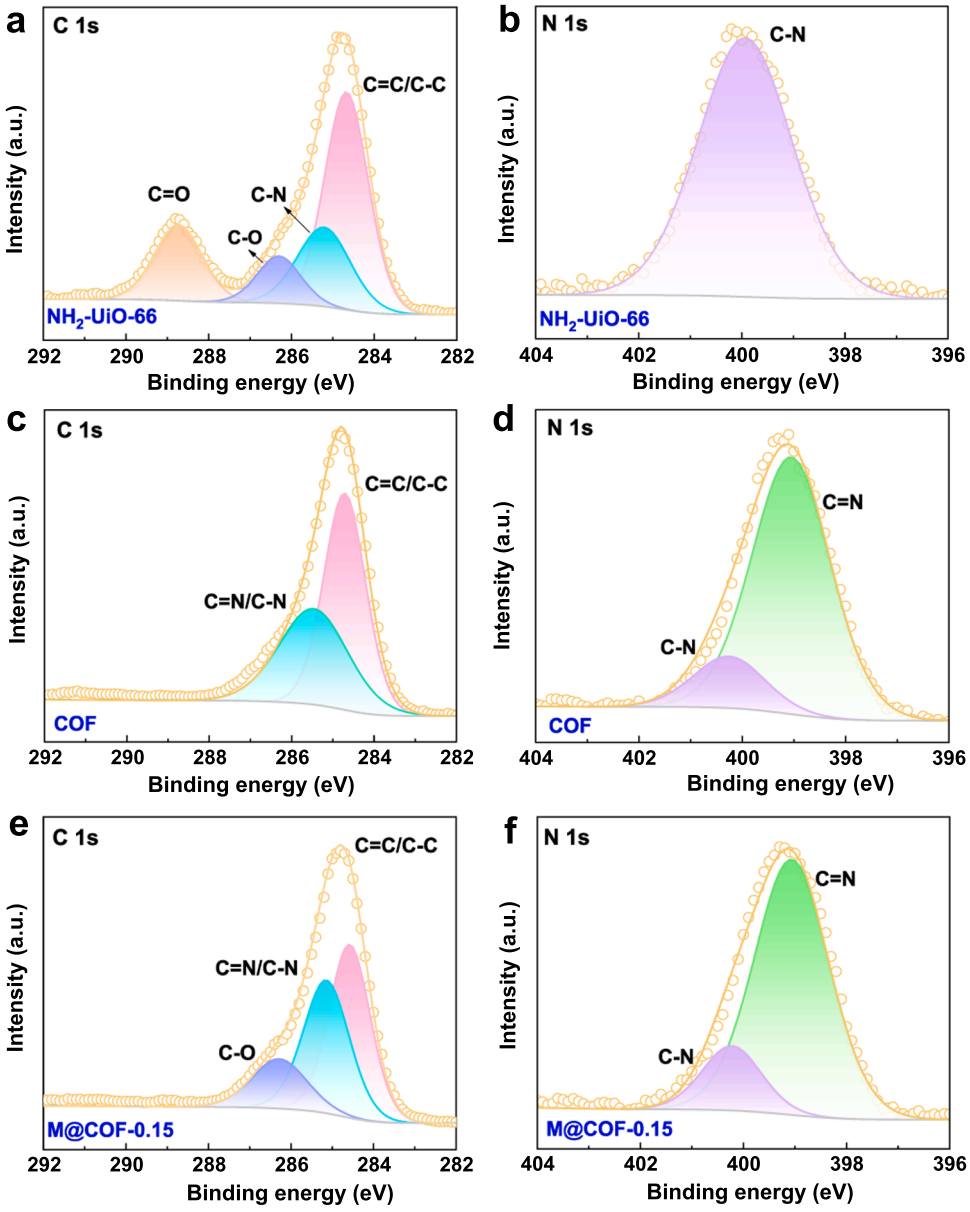

Fig. 3. High-resolution XPS of C 1 s and N 1 s of (a, b) NH_2-UiO-66; (c, d) COF; and (e, f) M@COF-0.15.

ranged from 0 to 1, suggesting a favorable adsorption process [42]. To examine the adsorption selectivity of the prepared materials, the N_2 adsorption curves at 273 K were investigated. The CO_2/N_2 adsorption selectivity was calculated, as shown in Fig. S3c. It was found that M@COF-0.15 exhibited the highest adsorption selectivity of 486, while the adsorption selectivity of M@COF-0.05 was slightly lower at 330 at 0.1 bar, CO_2 to N_2 of 10/90 v/v. This suggests that an appropriate thickness of the shell layer is advantageous for the selective separation of CO_2.

Considering that crucial role of adsorbent regeneration in practical applications, we thus assessed the regeneration performance of M@COF-0.05. Fig. 5a illustrates that the amount of CO_2 adsorption by M@COF-0.05 remains nearly constant after ten cycles of adsorption-desorption, indicating excellent regeneration performance. Additionally, the cycled M@COF-0.05 material was characterized to verify its structural integrity. A comparison of the N_2 adsorption-desorption curves and XRD results before and after cycling (Fig. 5b-c) revealed insignificant changes in the BET surface area and peak positions of the cycled materials, demonstrating the structural stability of the hybridized materials.

3.3. CO_2 conversion into cyclic carbonates

The conversion of CO_2 into high value-added chemicals is a promising method for utilizing CO_2. In this study, we used the materials prepared to synthesize cyclic carbonates through the cycloaddition reaction of CO_2 and allyl glycerol ether (AGE). Table 2 displays that both NH_2-UiO-66 and COF exhibit poor catalytic performance. Even the conversion of the hybridized M@COF-0.15 only reaches 12% (Entry 1–4). Given that pyridine-based COF offers advantages in terms of easy modification and functionalization, we used the PSM strategy to introduce bromoethanol into COF and M@COF-0.15. This allowed to obtain ion-functionalized COF-Br and M@COF-0.15-Br with active side chains for catalytic reactions. Interestingly, after bromine functionalization, the catalytic performance of COF-Br and M@COF-0.15-Br significantly improved, with the conversion of AGE increasing to 63–85% (Entry 5–6). To investigate the reason behind the improved catalytic performance of M@COF-0.15-Br, we conducted a reaction using pure NH_2-

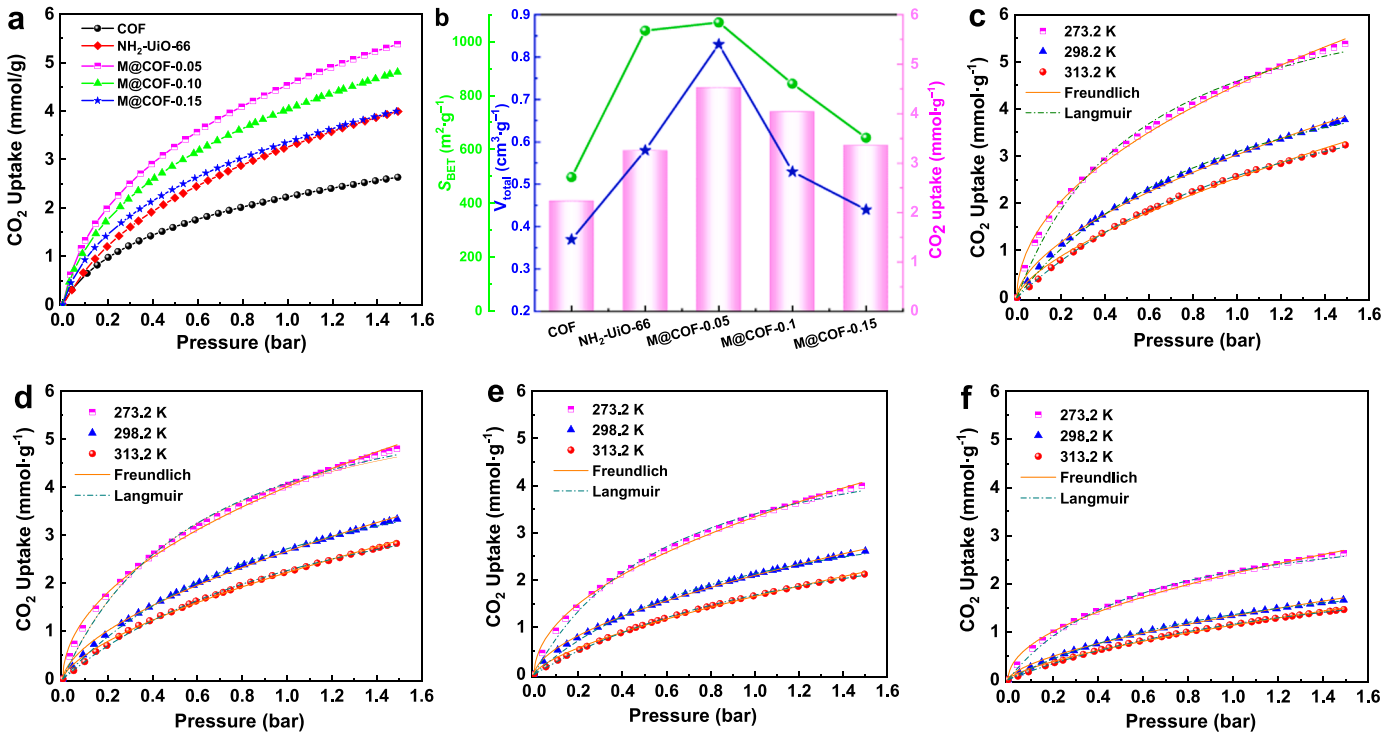

Fig. 4. Adsorption isotherms of CO_2 on NH_2-UiO-66, COF, and M@COF at 273 K; (b) relationship among surface area, total pore volume, and CO_2 uptake; CO_2 adsorption isotherms of (c) M@COF-0.05; (d) M@COF-0.10; (e) M@COF-0.15; (f) COF.

Table 1
Comparison of CO_2 adsorption capacity of the materials prepared in this work with adsorbents reported in the literature.[a].

Adsorbents	CO_2 uptake (mmol·g^{-1})	CO_2/N_2 selectivity	*Ref.*
NH_2-UiO-66 @Br-COF-4	3.85	40	[20]
MOF-74(Ni)– 8–140[b]	4.35	31	[46]
TMFPT-COF	1.71	36	[47]
ACOF-1	4.02	40	[48]
MIL-101(Cr)	3.26	8	[49]
MIL-101(Cr)-NH_2	3.00		[50]
Co-Al-LDH@Hf/Ti-MCP-AS[b]	2.57		[42]
HKUST-1/ANF-72[b]	7.29	39	[51]
PIL-NH_2 @MIL-101	2.23		[52]
NH_2-UiO-66	3.25		*This*
COF	2.23	103	*wok*
M@COF-0.05	4.53	126	
M@COF-0.10	4.04	153	
M@COF-0.15	3.36	150	

[a] Measured at 273 K and 1 bar. [b]Measured at 298 K and 1 bar

Table 2
Catalytic performance of various catalysts for CO_2 cycloaddition with AGE.

Entry	Catalysts	Conversion (%)	Selectivity
1	NH_2-UiO-66	3	99
2	COF	7	99
3	M@COF-0.05	11	99
4	M@COF-0.15	12	99
5	COF-Br	63	99
6	M@COF-0.15-Br	85	99
7	MOF+COF-Br[a]	64	99

Reaction conditions: catalysts (30 mg), allyl glycerol ether (AGE, 5 mmol), CO_2 (1.0 MPa), 120 °C, 12 h. [a]The physical mixing of NH_2-UiO-66 and COF-Br.

UiO-66 and COF-Br as catalyst through physical mixing. However, AGE conversion rate only reached 64% (Entry 7). This further confirms that the strategy of constructing core-shell material has a significant positive impact on the catalytic performance.

The effect of different reaction conditions on the M@COF-0.15-Br catalytic system was investigated, as shown in Fig. 6a. The yield of AGE increased from 44% to 94% when the reaction time was increased from 4 to 16 h, so the reaction 16 h was selected for further study from the perspective of high conversion rate. Similarly, the effect of different temperatures on AGE conversion was investigated and when the reaction temperature was increased from 80 to 120 °C, an increase in PC yield from 50% to 95% was observed (Fig. 6b). However, when the temperature was further increased to 140 °C, there was no significant increase in AGE conversion. Hence, the choice of 120 °C for the reaction was more appropriate from the point of view of energy conservation. The effects of different CO_2 pressure and catalyst dosage were also investigated, as shown in Fig. 6c-d. The AGE conversion increased insignificantly when the initial CO_2 pressure was increased from 1.0 to 2.0 MPa. With the increase of catalyst loading, the AGE conversion increased rapidly, achieving 51–98% conversion when using 10–30 mg of M@COF-0.15-Br. Further increases up to 40 mg is not significant for the cycloaddition reaction. Based on the optimization results of the above reaction parameters, we selected the optimal reaction conditions as follows: catalyst dosage of 30 mg, CO_2 pressure of 1.0 MPa, reaction temperature of 120 °C, and reaction time of 16 h.

With optimized conditions in hand, we evaluated the versatility of M@COF-0.15-Br for the cycloaddition of CO_2 and various epoxides. As shown in Scheme 2, the terminal epoxides reacted readily with CO_2 to produce cyclic carbonates with high yields and selectivity. In entries **1b-9b**, the epoxides with small spatial site resistance and electron-absorbing group substitution yielded higher product yields [53]. However, when styrene oxide was used as the substrate, the yield of **10b** slightly decreased to 91% due to the large spatial site resistance. It is important to note that when cyclohexene oxide was used as the reactant, the yield of **11b** was significantly lower at only 13%. This can be attributed to higher spatial resistance, which limited the nucleophilic

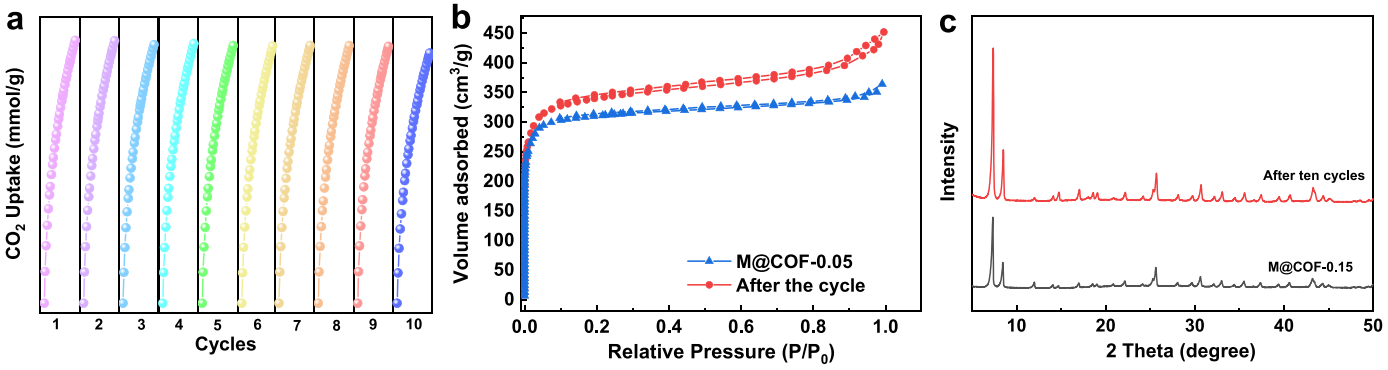

Fig. 5. (a) Ten cycles of CO_2 adsorption on M@COF-0.15; (b) N_2 adsorption-desorption curves before and after cycles; (c) XRD before and after cycles.

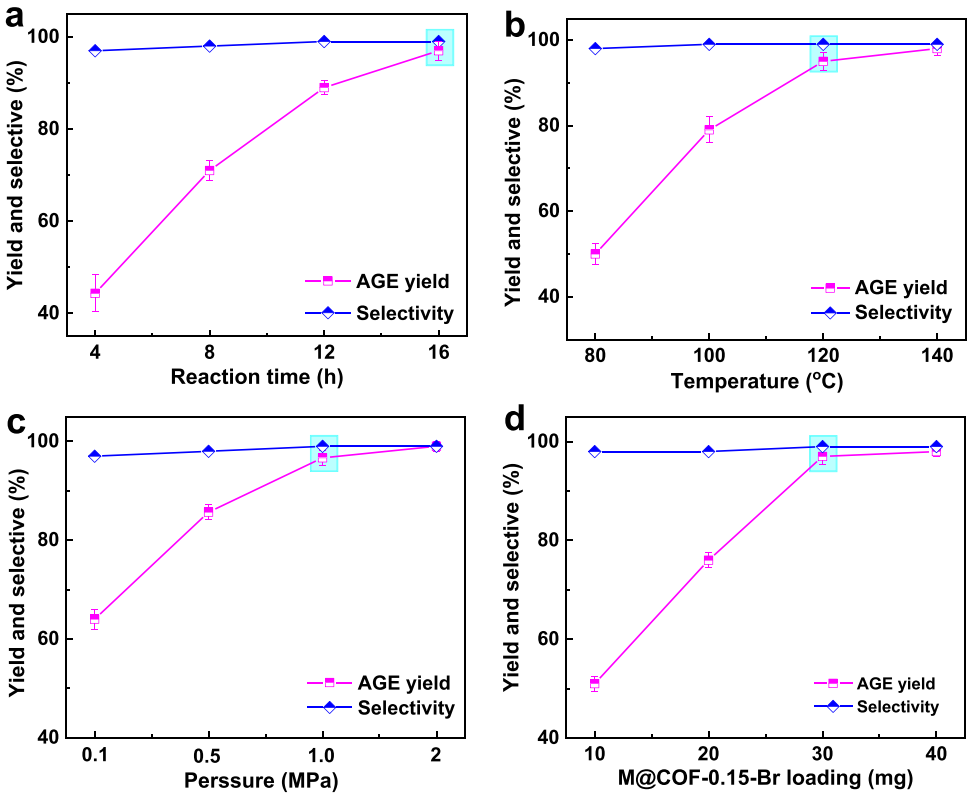

Fig. 6. (a) Effect of reaction time on the cycloaddition of CO_2 and AGE, conditions: catalyst 30 mg, AGE 10 mmol, 1.0 MPa, 120 °C; (b) reaction temperature, conditions: catalyst 30 mg, AGE 10 mmol, 1.0 MPa, 16 h; (c) CO_2 pressure, conditions: catalyst 30 mg, AGE 10 mmol, 120 °C, 16 h; (d) catalyst dosage, conditions: AGE 10 mmol, 120 °C, 1.0 MPa, 16 h.

attack of the Br^- ion and reduced the rate of ring opening [54,55]. After establishing the high catalytic activity of the M@COF-0.15-Br catalyst for terminal epoxides, we further investigated the more challenging coupling reaction of polyepoxides with CO_2 (**12b-17b**). Surprisingly, the epoxidation of several skeletons containing diglycidyl ethers resulted in successful conversion to bicyclic carbonates with yields ranging from 82% to 96%, without the need any additives and solvents. These findings further demonstrate the excellent catalytic performance of M@COF-0.15-Br.

The catalytic performance of the M@COF-0.15-Br was compared with similar materials reported in the literature (Table S3). It is evident to find that most of the reported COF catalysts require the addition of a numerous co-catalysts, such as TBAB, to achieve the conversion of CO_2 [56,57]. Although Py-Zn@IPOP was able to catalyzing the reaction without TBAB [58], the addition of metal to this COF increase its cost and operational complexity. Furthermore, although certain hybrid materials have shown progress in CO_2 catalytic reactions, they still face challenges such as the need for solvents, harsh reaction conditions, and poor CO_2 adsorption performance [59,60]. These issues greatly limit their practical applications. In contrast, the M@COF-0.15-Br materials prepared using a simple PSM strategy exhibited excellent CO_2 adsorption capacity and high cyclic carbonate yields during the catalytic conversion of CO_2. Importantly, this reaction does not require any co-catalysts, metals, and solvents. Therefore, M@COF-0.15-Br holds promise as a material for CO_2 capture and conversion.

To assess the stability of the catalyst, both leaching test and examined the effect of water content on the conversion of AGE were carried out, respectively. Fig. 7 demonstrates that even when the reaction was carried out up to 8 h and the catalyst was separated, there was minimal increase in after the filtrate was reintroduced to the reaction. This suggests that the catalyst's active component remains intact during the reaction. As industries typically emit large quantities of water along

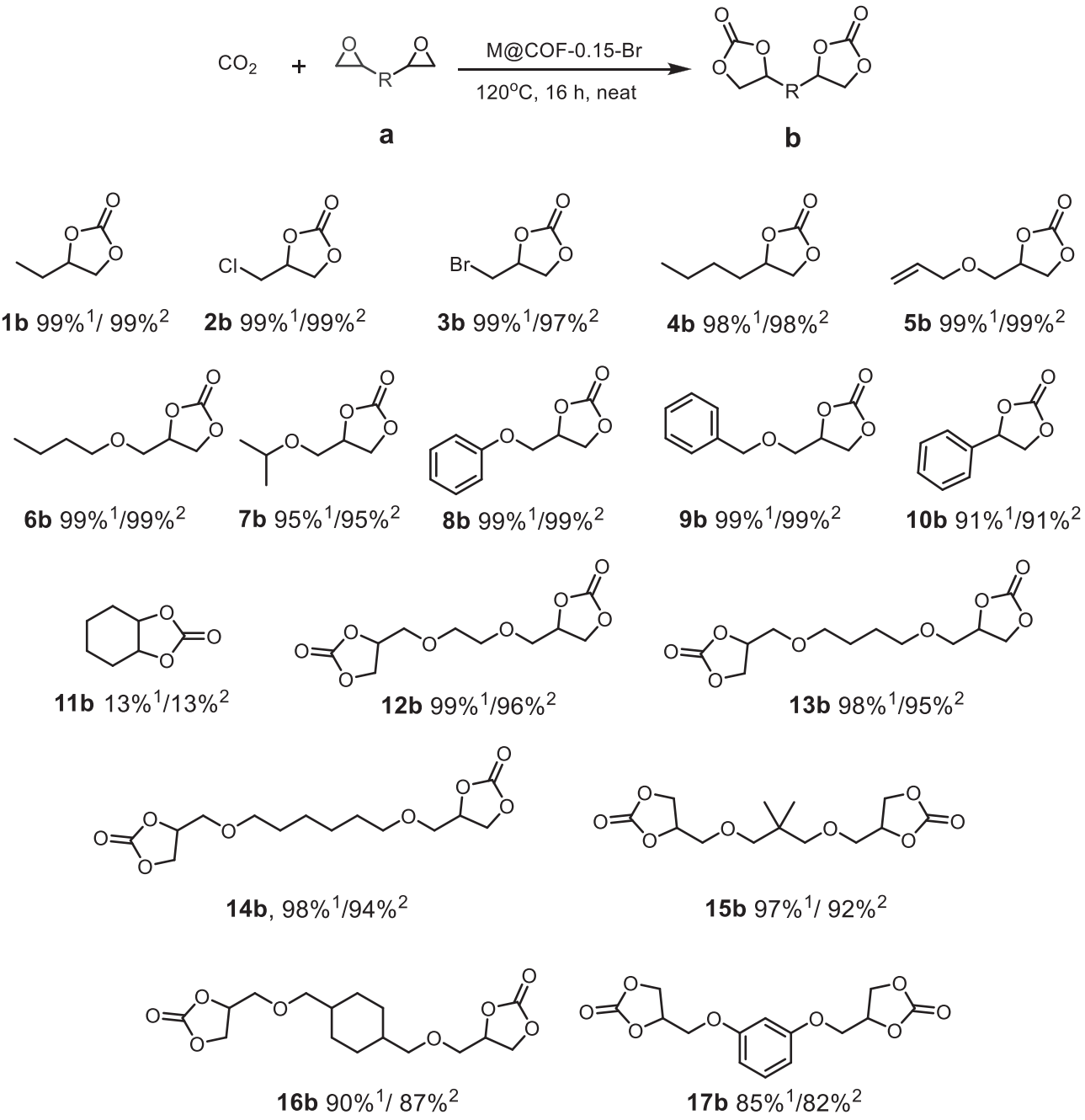

Scheme 2. Synthesis of various cyclic carbonates catalyzed by M@COF-0.15-Br. Reaction conditions: epoxide (5 mmol), CO_2 (1.0 MPa), [1]The conversion of epoxide was determined by ^{1}H NMR. [2]The yield of cyclic carbonate was determined by ^{1}H NMR.

with CO_2, it is crucial to investigate how water affects product yields in catalyst systems. Fig. 7b illustrates that the conversion of AGE tends to decrease as the water content in the catalytic system increases. However, even when the water content increases to 20 mol%, the conversion of AGE remains above 82%. This indicates the potential practical application of M@COF-0.15-Br.

3.4. Kinetic investigation of CO_2 conversion

During the optimization process, we observed significantly variation in the conversion of AGE as reaction time and temperature increased. Consequently, a set of kinetic reaction experiments were conducted to validate the impact of various on the conversion of AGE. To determine the activation energy of the reaction, we explored the temperature dependence of the reaction and derived simplified kinetic equations based on existing literature reports [61–63]:

$$\ln(1-x) = -k_{obs}t + C \quad (1)$$

$$\ln k_{obs} = -Ea/RT + A \quad (2)$$

where k_{obs} is the rate constant, t is the reaction time (h), x is the AGE conversion (%), T is the temperature (K), A is the pre-exponential factor (s^{-1}), and Ea is the activation energy ($J{\cdot}mol^{-1}$).

The kinetics of the reaction were investigated using Eq. (1), and the rate constants (k_{obs}) were determined by analyzing the slope of the linear relationship between ln(1-x) and time (t). The resulting experimental data can be found in Fig. S4. Notably, all conditions yielded correlation coefficients with squared values close to 1, indicating a

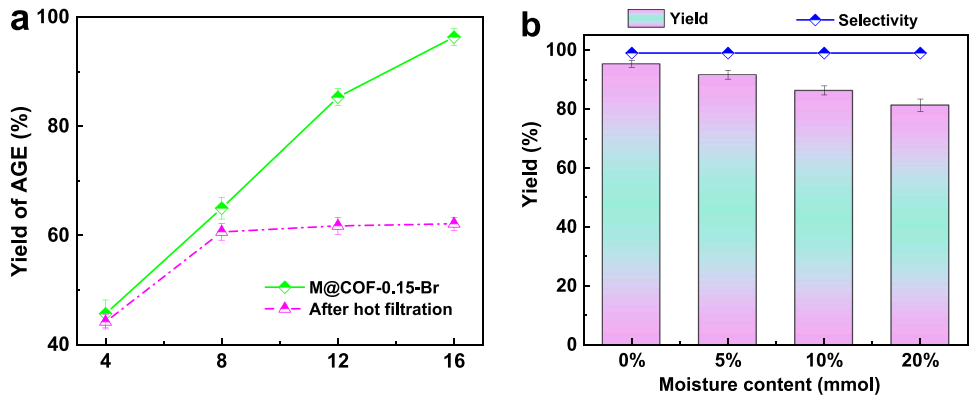

Fig. 7. Leaching test of M@COF-0.15-Br and the effect of water content on the cycloaddition of CO_2 and AGE.

strong indication that the reaction is a first-order process concerning AGE concentration, catalyst dosage, and CO_2 pressure.

To investigate the superiority of the M@COF-0.15-Br hybrid material over COF-Br, the dynamic processes and activation energies of the catalytic AGE were examined at different temperatures (80 °C, 100 °C, 120 °C, and 140 °C) for both catalysts. By comparing of Fig. 8a and b, it is evident the M@COF-0.15-Br exhibits higher conversion and a larger k_{obs} under the same conditions. This indicates that M@COF-0.15-Br is more favorable for the catalytic reaction from a kinetic perspective. The activation energies of the reactions were calculated using the Arrhenius equation to be 43 kJ·mol^{-1} for COF-Br and 35 kJ·mol^{-1} for M@COF-0.15-Br (Fig. 8c). Notably, M@COF-0.15-Br has a lower energy barrier for the cycloaddition reaction of AGE and CO_2. This can be attributed to its well-developed porous structure, CO_2 adsorption sites, and the structural synergies generated at the core-shell interface [64], which effectively promote the efficient conversion of CO_2.

3.5. Reusability of M@COF-0.15-Br

Cycling experiments were conducted to assess the reusability and durability of M@COF-0.15-Br. Six regeneration experiments were conducted using AGE as the substrate (Fig. 9a). Despite a slight decrease in catalyst activity, a product yield of over 95% was consistently achieved after six cycles (Fig. S5 shows the ^{1}H NMR of the reaction products). These findings demonstrate the excellent catalytic cycle stability of M@COF-0.15-Br. Importantly, M@COF-0.15-Br can be readily recovered from the system through centrifugation. Additionally, the structure was characterized to investigate its stability following the catalytic reaction. The FTIR spectra of M@COF-0.15-Br show no significant change before and after cycling (Fig. 9b). Furthermore, the crystal structure of the recycled catalyst closely resembles that of the initial M@COF-0.15-Br (Fig. 9c). Notably, TGA analysis reveals a partial weight loss after recycling (Fig. 9d), possibly due to the residual cyclic carbonate. These

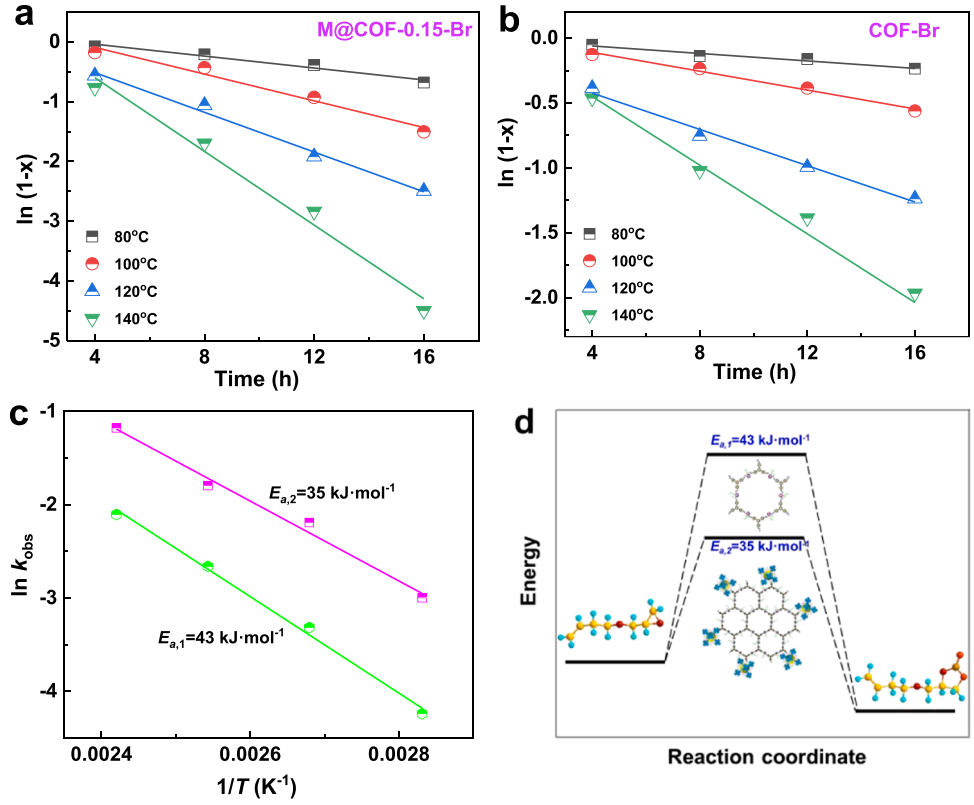

Fig. 8. First-order kinetic plots ln(1-x) versus time at different temperatures (a) M@COF-0.15-Br; (b) COF-Br; (c) the fitting curve of the natural logarithm of the observed first order rate constant (lnk_{obs}) against the reciprocal of absolute 1/T; (d) the apparent activate energies of COF-Br and M@ −0.15-Br.

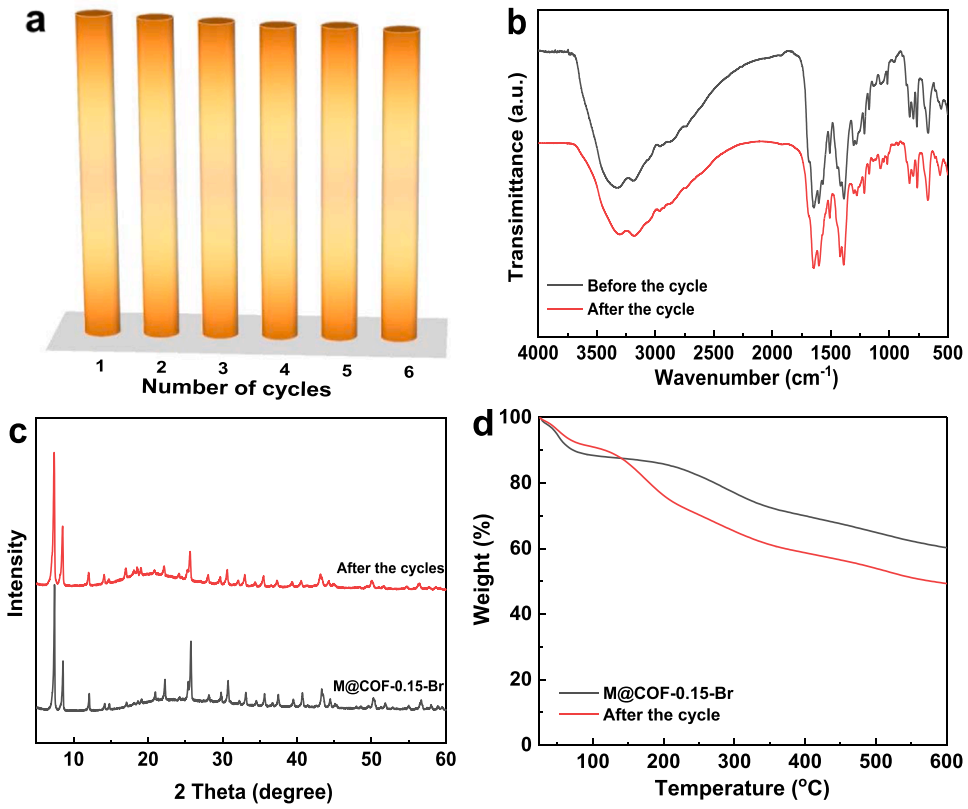

Fig. 9. (a) Reusability of M@COF-0.15-Br; characterization of M@COF-0.15-Br before and after cycling (b) FTIR spectra; (c) XRD pattern; and (d) TGA curves.

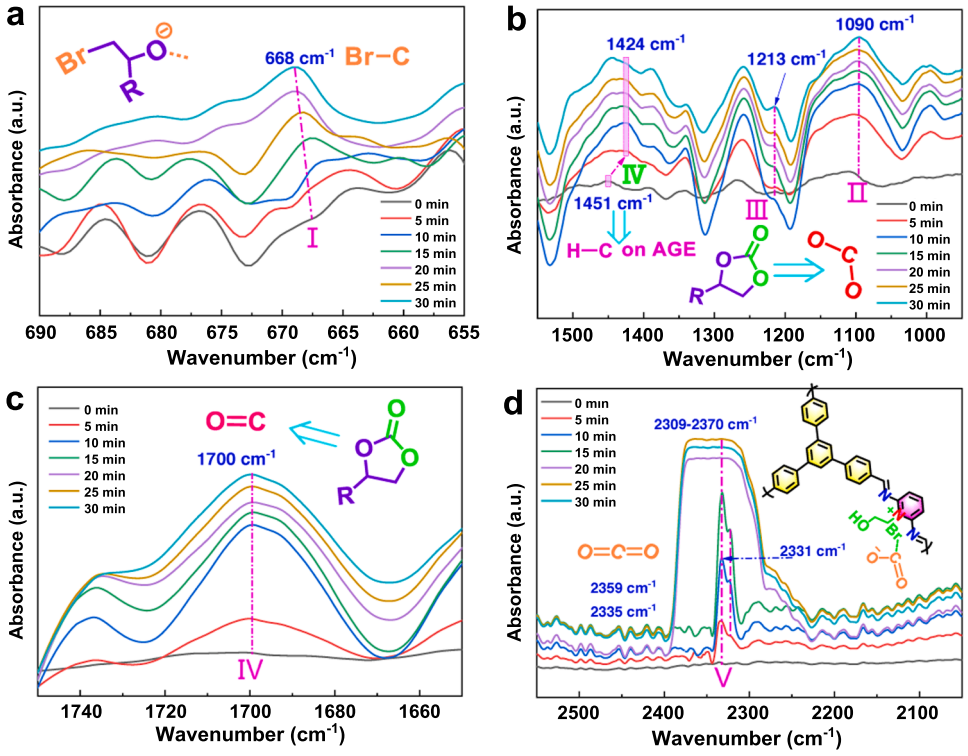

Fig. 10. *In-situ* FTIR spectra of the reaction of AGE with CO_2 at different reaction times using M@COF-0.15-Br as catalyst at atmospheric pressure and 120 °C (CO_2 flow rate: 10 mL·min^{-1}).

finding demonstrate that M@COF-0.15-Br is an efficient and easily recoverable catalyst for the CO_2 cycloaddition reaction.

3.6. Catalytic mechanism research

To elucidate the catalytic mechanism of the cycloaddition process, the reactions of CO_2 and AGE at different reaction times were analyzed using in situ FTIR. As shown in Fig. 10a, the C-Br stretching vibration peak at 668 cm^{-1} gradually strengthens with increasing reaction time, suggesting that Br^- acts as a nucleophile to attacking the less hindered carbon atoms on the epoxide ring, thereby facilitating the ring opening process of the epoxide [65]. Notably, distinct pecks at 1090 and 1213 cm^{-1} (Fig. 10b) are generated in the presence of a catalyst, which correspond to the C-O-C stretching vibrations of the resulting carbonate product [66,67]. Furthermore, the stretching vibration peak of C═O on the carbonate is detected at 1700 cm^{-1} (Fig. 10c), indicating the smooth progression of cycloaddition process and successful conversion of epoxide and CO_2 into cyclic carbonate [68]. It is recognized that the activation of inert CO_2 is crucial for facilitating its conversion. The in situ FTIR spectrum in Fig. 10d demonstrates the adsorption capacity of M@COF-0.15-Br on CO_2. Here a characteristic peak of CO_2 appears within the range of 2309–2370 cm^{-1}, accompanied by a strong vibrational peak and shoulder peak at 2331 cm^{-1}, indicating a strong interaction between CO_2 and Br^- ion [69].

Based on the results of in situ FTIR experiments, a feasible mechanism is proposed in Fig. 11. Initially, Zr coordinatively unsaturated sites (CUS), which acts Lewis acid site, interacts with the oxygen of the epoxide through electrophilic interactions, causing polarization of the epoxide ring [70]. Simultaneously, hydrogen bonds are formed between the hydrogen atom in the hydroxyl group of the catalyst and the oxygen atom of the epoxide, activating the epoxide [71,72]. Subsequently, the nucleophilic Br^- anion from the catalyst attacks the β-carbon atom, initiating a ring-opening process of the epoxide to form a bromoalkoxy complex. After that, CO_2 is inserted into the complex, resulting in the formation of a bromocarbonate complex [73]. Finally, the ring undergoes intramolecular closure, resulting in the formation of a cyclic carbonate and the regeneration of the catalyst.

4. Conclusions

In summary, a series of hybrid materials called M@COFs were successfully prepared by in-situ growing of pyridine-based COF shell layers with different thicknesses onto the surface of NH_2-UiO-66(Zr) cores. These M@COFs possess strong synergistic properties and also inherit the excellent characteristics of the parent MOF and COF, including high surface area, stable physicochemical properties, π-π stacking interactions, and easily modifiable structures. Notably, M@COFs have abundant Lewis base sites (Zr) and π-π stacking interactions, which contribute to their exceptional CO_2 adsorption and selectivity. Among them, M@COF-0.05 exhibited the highest CO_2 uptake of 4.53 $mmol \cdot g^{-1}$ at 273 K and 1 bar, surpassing that of most other MOFs of COFs materials. Additionally, a simple PSM strategy was developed to prepare ion-functionalized M@COF-0.15-Br with active side chains for the cycloaddition reaction of CO_2 and epoxides. The ion-functionalization treatment enriches the ion active sites on the surface of the shell layer, while the core-shell interface produces synergistic effects, effectively promoting the conversion of CO_2 into monocyclic and polycyclic carbonates. Furthermore, the activation energy demonstrate that the energy barrier required for the catalytic conversion of M@COF-0.15-Br (35 $kJ \cdot mol^{-1}$) is significantly lower than that of pure COF-Br (45 $kJ \cdot mol^{-1}$), indicating favorable reaction kinetics for M@COF-0.15-Br. Moreover, the M@COF-0.15-Br catalyst can be easily separated through simple centrifugation and maintain negligible loss of activity after six cycles. Consequently, the M@COF hybrid materials are deemed as attractive candidates for CO_2 capture and conversion.

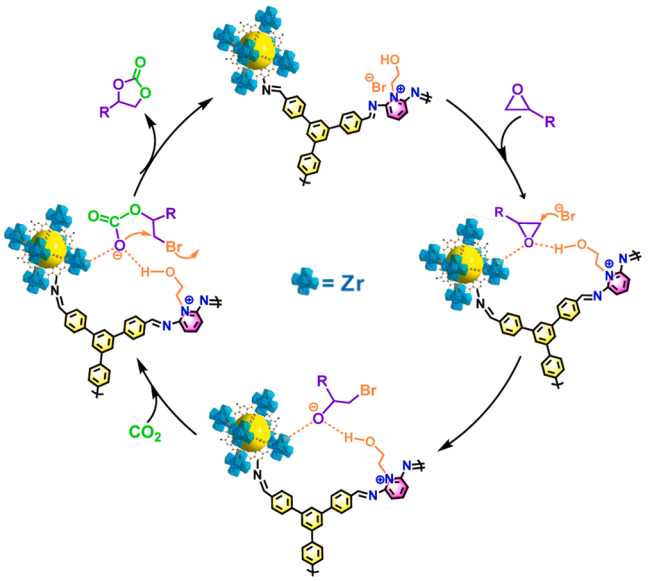

Fig. 11. Proposed reaction mechanism for the cycloaddition of CO_2 and epoxides over M@COF-0.15-Br.

CRediT authorship contribution statement

Ping Liu: Investigation, Writing – original draft. **Kaixing Cai:** Investigation, Writing – original draft. **Duan-Jian Tao**: Supervision, Project administration. **Tianxiang Zhao:** Writing – review & editing, Conceptualization, Supervision, Funding acquisition.

Declaration of Competing Interest

The authors declare that they have no known competing financial interests or personal relationships that could have appeared to influence the work reported in this paper.

Data availability

Data will be made available on request.

Acknowledgment

This work was supported by the National Natural Science Foundation of China (nos. 22168012 and 22208070). We would like to thank the researchers in the Shiyanjia Lab (www.shiyanjia.com) for their helping with TEM and ^{13}C CP-MAS NMR analysis.

Appendix A. Supporting information

Supplementary data associated with this article can be found in the online version at doi:10.1016/j.apcatb.2023.123317.

References

[1] H.C. Gulbalkan, Z.P. Haslak, C. Altintas, A. Uzun, S. Keskin, Assessing CH_4/N_2 separation potential of MOFs, COFs, IL/MOF, MOF/Polymer, and COF/Polymer composites, Chem. Eng. J. 428 (2022), 131239.
[2] I.W. Almanassra, L. Jaber, A. Chatla, A. Abushawish, A. Shanableh, M. Ali Atieh, Unveiling the relationship between MOF porosity, particle size, and polyethersulfone membranes properties for efficient decontamination of dye and organic matter, Chem. Eng. J. 471 (2023), 144616.
[3] G. Yuan, L. Tan, P. Wang, Y. Wang, C. Wang, H. Yan, Y.-Y. Wang, MOF-COF composite photocatalysts: design, synthesis, and mechanism, Cryst. Growth Des. 22 (2021) 893–908.
[4] R. Luo, Y. Yang, K. Chen, X. Liu, M. Chen, W. Xu, B. Liu, H. Ji, Y. Fang, Tailored covalent organic frameworks for simultaneously capturing and converting CO_2 into cyclic carbonates, J. Mater. Chem. A 9 (2021) 20941–20956.

[5] R. Zheng, W. Yan, Y. Xia, Highly water-dispersible hydroxyl functionalized covalent organic frameworks as matrix for enhanced MALDI-TOF MS identification and quantification of quaternary ammonium salts in water and fruits, Anal. Chim. Acta 1227 (2022), 340269.
[6] R. Liu, K.T. Tan, Y. Gong, Y. Chen, Z. Li, S. Xie, T. He, Z. Lu, H. Yang, D. Jiang, Covalent organic frameworks: an ideal platform for designing ordered materials and advanced applications, Chem. Soc. Rev. 50 (2021) 120–242.
[7] D. Ma, Y. Song, H. Zhao, C. Yu, Y. Zhang, C. Li, K. Liu, Ordered macro–microporous covalent organic frameworks as bifunctional catalysts for CO_2 cycloaddition, ACS Sustain. Chem. Eng. 11 (2023) 6183–6190.
[8] X. Xu, N. Zhang, Y. Gao, T. Bao, S. Wang, MOF@COF functionalized cotton fiber as a platform for high performance extraction and removal of bisphenols from water samples, J. Environ. Chem. Eng. 10 (2022), 107072.
[9] M.Y. Zhang, J.K. Li, R. Wang, S.N. Zhao, S.Q. Zang, T.C.W. Mak, Construction of core-Shell MOF@COF hybrids with controllable morphology adjustment of COF shell as a novel platform for photocatalytic cascade reactions, Adv. Sci. 8 (2021), e2101884.
[10] D. Sun, S. Jang, S. Yim, L. Ye, D. Kim, Metal doped core-shell metal-organic frameworks@covalent organic frameworks (MOFs@COFs) hybrids as a novel photocatalytic platform, Adv. Funct. Mater. 28 (2018) 1707110.
[11] R. Li, J. Yan, B. Feng, M. Sun, C. Ding, H. Shen, J. Zhu, S. Yu, Ultrasensitive detection of multidrug-resistant bacteria based on boric acid-functionalized fluorescent MOF@COF, ACS Appl. Mater. Interfaces 15 (2023) 18663–18671.
[12] H. Zhang, Y. Yang, C. Li, H. Tang, F. Zhang, G. Zhang, H. Yan, A new strategy for constructing covalently connected MOF@COF core–shell heterostructures for enhanced photocatalytic hydrogen evolution, J. Mater. Chem. A 9 (2021) 16743–16750.
[13] F.M. Zhang, J.L. Sheng, Z.D. Yang, X.J. Sun, H.L. Tang, M. Lu, H. Dong, F.C. Shen, J. Liu, Y.Q. Lan, Rational design of MOF/COF hybrid materials for photocatalytic H_2 evolution in the presence of sacrificial electron donors, Angew. Chem. Int. Ed. 57 (2018) 12106–12110.
[14] Q.Q. Xia, X.H. Wang, J.L. Yu, Z.Y. Xue, J. Chai, X. Liu, M.X. Wu, Tale of COF-on-MOF composites with structural regulation and stepwise luminescence enhancement, ACS Appl. Mater. Interfaces 14 (2022) 45669–45678.
[15] Y. Liu, H. Wu, R. Li, J. Wang, Y. Kong, Z. Guo, H. Jiang, Y. Ren, Y. Pu, X. Liang, F. Pan, Y. Cao, S. Song, G. He, Z. Jiang, MOF-COF "Alloy" membranes for efficient propylene/propane separation, Adv. Mater. 34 (2022), e2201423.
[16] Y. Li, L. Liu, T. Meng, L. Wang, Z. Xie, Structural engineering of ionic MOF@COF heterointerface for exciton-boosting sunlight-driven photocatalytic filter, ACS Nano 17 (2023) 2932–2942.
[17] H. Peng, J. Raya, F. Richard, W. Baaziz, O. Ersen, A. Ciesielski, P. Samori, Synthesis of robust MOFs@COFs porous hybrid materials via an aza-diels-alder reaction: towards high-performance supercapacitor Materials, Angew. Chem. Int. Ed. 59 (2020) 19602–19609.
[18] M. Cai, Y. Li, Q. Liu, Z. Xue, H. Wang, Y. Fan, K. Zhu, Z. Ke, C.Y. Su, G. Li, One-Step construction of hydrophobic MOFs@COFs core-shell composites for heterogeneous selective catalysis, Adv. Sci. 6 (2019) 1802365.
[19] G. Lu, X. Huang, Y. Li, G. Zhao, G. Pang, G. Wang, Covalently integrated core-shell MOF@COF hybrids as efficient visible-light-driven photocatalysts for selective oxidation of alcohols, J. Energy Chem. 43 (2020) 8–15.
[20] J. Wang, L. Wang, Y. Wang, F. Yang, J. Li, X. Guan, J. Zong, F. Zhou, J. Huang, Y.-N. Liu, Covalently connected core–shell NH_2-UiO-66@Br-COFs hybrid materials for CO_2 capture and I_2 vapor adsorption, Chem. Eng. J. 438 (2022), 135555.
[21] Y. Cheng, Y. Ying, L. Zhai, G. Liu, J. Dong, Y. Wang, M.P. Christopher, S. Long, Y. Wang, D. Zhao, Mixed matrix membranes containing MOF@COF hybrid fillers for efficient CO_2/CH_4 separation, J. Membr. Sci. 573 (2019) 97–106.
[22] K. Li, N.K. Wong, M.J. Strauss, A.M. Evans, M. Matsumoto, W.R. Dichtel, A. Adronov, Postsynthetic modification of a covalent organic framework achieved via strain-promoted cycloaddition, J. Am. Chem. Soc. 143 (2021) 649–656.
[23] Y.J. Chen, H.Y. Zhuo, Y. Pan, J.X. Liang, C.G. Liu, J. Li, Triazine COF-supported single-atom catalyst (Pd1/trzn-COF) for CO oxidation, Sci. China Mater. 64 (2021) 1939–1951.
[24] Y. Peng, M. Zhao, B. Chen, Z. Zhang, Y. Huang, F. Dai, Z. Lai, X. Cui, C. Tan, H. Zhang, Hybridization of MOFs and COFs: a new strategy for construction of MOF@COF core-shell hybrid materials, Adv. Mater. 30 (2018) 1705454.
[25] X.Y. Wang, H.Q. Yin, X.B. Yin, MOF@COFs with strong multiemission for differentiation and ratiometric fluorescence detection, ACS Appl. Mater. Interfaces 12 (2020) 20973–20981.
[26] C. Mao, K. Yin, C. Yang, G. Dong, G. Tian, Y. Zhang, Y. Zhou, Fe-based MOFs@Pd@COFs with spatial confinement effect and electron transfer synergy of highly dispersed Pd nanoparticles for Suzuki-Miyaura coupling reaction, J. Colloid Interface Sci. 608 (2022) 809–819.
[27] C. Li, X. Xu, J. Xing, F. Wang, Y. Shi, X. Zhao, J. Liu, Y. Yang, Z. Zhao, A fluorescent dual-emissions UiO-66-NH_2@TpTt-COF core-shell composite for sensitive and optosmart sensing of tetracycline, Appl. Surf. Sci. 616 (2023), 156455.
[28] Q. Yang, Y. Zhang, N. Ding, Q. Hu, X. Yan, J. Liu, P. Zhang, S. Fu, Q. Wang, L. Wu, S. Wu, A stable MOF@COF-Pd catalyst for C–C coupling reaction of pyrimidine sulfonate and arylboronic acid, Appl. Organomet. Chem. 36 (2022), e6775.
[29] Q. Liao, C. Ke, X. Huang, D. Wang, Q. Han, Y. Zhang, Y. Zhang, K. Xi, A versatile method for functionalization of covalent organic frameworks via suzuki–miyaura cross-coupling, Angew. Chem. Int. Ed. 60 (2020) 1411–1416.
[30] Y. Wang, J. Zhao, S. Zhang, Z. Zhang, Z. Zhu, M. Wang, B. Lyu, G. He, F. Pan, Z. Jiang, Two-step fabrication of COF membranes for efficient carbon capture, Mater. Horiz. (2023).
[31] X. N, Y. Yang, X. Cao, T. Wang, D.M. Kong, X.B. Yin, B. Li, X.H. Bu, General approach to construct C-C single bond-linked covalent organic frameworks, J. Am. Chem. Soc. (2023), https://doi.org/10.1021/jacs.3c05403.
[32] S. Haldar, K. Roy, R. Kushwaha, S. Ogale, R. Vaidhyanathan, Chemical exfoliation as a controlled route to enhance the anodic performance of COF in LIB, Adv. Energy Mater. 9 (2019) 1902428.
[33] Y. He, N. An, C. Meng, K. Xie, X. Wang, X. Dong, D. Sun, Y. Yang, Z. Hu, High-density active site COFs with a flower-like morphology for energy storage applications, J. Mater. Chem. A 10 (2022) 11030–11038.
[34] H. Zhang, Q. Zhu, R. Yuan, H. He, Crystal engineering of MOF@COF core-shell composites for ultra-sensitively electrochemical detection, Sens. Actuators B Chem. 329 (2021), 129144.
[35] K. Wang, Z. Jia, Y. Bai, X. Wang, S.E. Hodgkiss, L. Chen, S.Y. Chong, X. Wang, H. Yang, Y. Xu, F. Feng, J.W. Ward, A.I. Cooper, Synthesis of stable thiazole-linked covalent organic frameworks via a multicomponent reaction, J. Am. Chem. Soc. 142 (2020) 11131–11138.
[36] T. Zhang, S. Liu, X. Zhang, J. Gao, H. Yu, Q. Ye, S. Liu, W. Liu, Fabrication of two-dimensional functional covalent organic frameworks via the thiol-ene "click" reaction as lubricant additives for antiwear and friction reduction, ACS Appl. Mater. Interfaces 13 (2021) 36213–36220.
[37] F. Li, D. Wang, Q. Xing, G. Zhou, S. Liu, Y. Li, L. Zheng, P. Ye, J. Zou, Design and syntheses of MOF/COF hybrid materials via postsynthetic covalent modification: an efficient strategy to boost the visible-light-driven photocatalytic performance, Appl. Catal. B Environ. 243 (2019) 621–628.
[38] Y. Chen, D. Yang, B. Shi, W. Dai, H. Ren, K. An, Z. Zhou, Z. Zhao, W. Wang, Z. Jiang, In situ construction of hydrazone-linked COF-based core–shell hetero-frameworks for enhanced photocatalytic hydrogen evolution, J. Mater. Chem. A 8 (2020) 7724–7732.
[39] W. Shi, H. Wang, J. Yan, L. Shan, G. Quan, X. Pan, L. Cui, Wheat straw derived biochar with hierarchically porous structure for bisphenol A removal: Preparation, characterization, and adsorption properties, Sep. Purif. Technol. 289 (2022), 120796.
[40] J. Shi, H. Cui, J. Xu, N. Yan, S. You, Synthesis of N-doped hierarchically ordered micro-mesoporous carbons for CO_2 adsorption, J. CO_2 Util. 62 (2022), 102081.
[41] P. Puthiaraj, S. Ravi, K. Yu, W. Ahn, CO_2 adsorption and conversion into cyclic carbonates over a porous $ZnBr_2$-grafted N-heterocyclic carbene-based aromatic polymer, Appl. Catal. B Environ. 251 (2019) 195–205.
[42] Z. Huang, L. Ying, F. Gong, S. Liu, W. Wang, J. Ding, MOF-derived bimetallic coordination polymer@cobalt-aluminum layered double hydroxide for highly selective CO_2 adsorption: experiments, mechanisms, J. Colloid Interface Sci. 645 (2023) 784–793.
[43] R. Ping, C. Ma, Z. Shen, G. Zhang, D. Wang, F. Liu, M. Liu, Metalloporphyrin and triazine integrated nitrogen-rich frameworks as high-performance platform for CO_2 adsorption and conversion under ambient pressure, Sep. Purif. Technol. 310 (2023), 123151.
[44] S. Roy, B. Dasgupta Ghosh, K. Lim Goh, H. Jun Ahn, Y.W. Chang, Super expanded freestanding 3D graphene foam as a versatile platform for CO_2 capture and hydrogenation, Chem. Eng. J. 466 (2023), 143326.
[45] A. Mukhtar, S. Saqib, N.B. Mellon, S. Rafiq, M. Babar, S. Ullah, N. Muhammad, A. L. Khan, M. Ayoub, M. Ibrahim, K. Maqsood, M.A. Bustam, A.G. Al-Sehemi, J. J. Klemeš, S. Asif, A. Bokhari, A review on CO_2 capture via nitrogen-doped porous polymers and catalytic conversion as a feedstock for fuels, J. Clean. Prod. 277 (2020), 123999.
[46] L. Lei, Y. Cheng, C. Chen, M. Kosari, Z. Jiang, C. He, Taming structure and modulating carbon dioxide (CO_2) adsorption isosteric heat of nickel-based metal organic framework (MOF-74(Ni)) for remarkable CO_2 capture, J. Colloid Interface Sci. 612 (2022) 132–145.
[47] X. Li, Q. Su, K. Luo, H. Li, G. Li, Q. Wu, Construction of a highly heteroatom-functionalized covalent organic framework and its CO_2 capture capacity and CO_2/N_2 selectivity, Mater. Lett. 282 (2021), 128704.
[48] Z. Li, X. Feng, Y. Zou, Y. Zhang, H. Xia, X. Liu, Y. Mu, A 2D azine-linked covalent organic framework for gas storage applications, Chem. Commun. 50 (2014) 13825–13828.
[49] R. Zhong, X. Yu, W. Meng, J. Liu, C. Zhi, R. Zou, Amine-grafted MIL-101(Cr) via double-solvent incorporation for synergistic enhancement of CO_2 uptake and selectivity, ACS Sustain. Chem. Eng. 6 (2018) 16493–16502.
[50] D. Jiang, L.L. Keenan, A.D. Burrows, K.J. Edler, Synthesis and post-synthetic modification of MIL-101(Cr)-NH_2 via a tandem diazotisation process, Chem. Commun. 48 (2012) 12053–12055.
[51] G. Zhao, Z. Li, B. Cheng, X. Zhuang, T. Lin, Hierarchical porous metal organic framework aerogel for highly efficient CO_2 adsorption, Sep. Purif. Technol. 315 (2023), 123754.
[52] Y. Jiang, D. Li, Y. Zhao, J. Sun, Hydrogen bond donor functionalized poly(ionic liquids)@MIL-101 for the CO_2 capture and improving the catalytic CO_2 conversion with epoxide, J. Colloid Interface Sci. 618 (2022) 22–33.
[53] C. Li, W. Xiong, T. Zhao, F. Liu, H. Cai, P. Chen, X. Hu, Mechanochemical construction of mesoporous silicon-supported organocatalysts with alkylol-amine cooperative sites for CO_2 fixation into cyclic carbonates under halogen-free conditions, Appl. Catal. B Environ. 324 (2023), 122217.
[54] F. Liu, S. Du, W. Zhang, J. Ma, S. Wang, M. Liu, F. Liu, Construction of zwitterionic porous organic frameworks with multiple active sites for highly efficient CO_2 adsorption and synergistic conversion, Chem. Eng. J. 435 (2022), 134921.
[55] M. Liu, P. Zhao, R. Ping, F. Liu, F. Liu, J. Gao, J. Sun, Squaramide-derived framework modified periodic mesoporous organosilica: a robust bifunctional platform for CO_2 adsorption and cooperative conversion, Chem. Eng. J. 399 (2020), 125682.

[56] H. Lia, X. Feng, P. Shao, J. Chen, C. Li, S. Jayakumarad, Q. Yang, Synthesis of covalent organic frameworks via in situ salen skeleton formation for catalytic applications, J. Mater. Chem. A 7 (2019) 5482–5492.
[57] J. Cao, W. Shan, Q. Wang, X. Ling, G. Li, Y. Lyu, Y. Zhou, J. Wang, Ordered porous poly(ionic liquid) crystallines: spacing confined ionic surface enhancing selective CO_2 capture and fixation, ACS Appl. Mater. Interfaces 11 (2019) 6031–6041.
[58] W. Zhang, R. Ping, X. Lu, H. Shi, F. Liu, J. Ma, M. Liu, Rational design of Lewis acid-base bifunctional nanopolymers with high performance on CO_2/epoxide cycloaddition without a cocatalyst, Chem. Eng. J. 451 (2023), 138715.
[59] M. Ding, H.L. Jiang, Incorporation of imidazolium-based poly(ionic liquid)s into a metal–organic framework for CO_2 Capture and conversion, ACS Catal. 8 (2018) 3194–3201.
[60] Y.R. Du, X. Yang, Y.F. Wang, P.X. Guan, R. Wang, B.H. Xu, Immobilization poly (ionic liquid)s into hierarchical porous covalent organic frameworks as heterogeneous catalyst for cycloaddition of CO_2 with epoxides, Mol. Catal. 520 (2022), 112164.
[61] K. Cai, P. Liu, Z. Chen, P. Chen, F. Liu, T. Zhao, D.J. Tao, Construction of bifunctional triazine-based imidazolium porous ionomer polymers by a post-crosslinking tactic for efficient CO_2 capture and conversion, Chem. Eng. J. 451 (2023), 138946.
[62] P. Liu, K. Cai, M. Liu, F. Liu, P. Chen, T. Zhao, Exceptionally effective H_2S absorption and conversion into thiols in novel superbase protic ionic liquids, AlChE J. 69 (2023) 17944.
[63] N. Li, S. Qin, Y. Hao, X. Wang, T. Chang, X. Liu, Y. Zhang, B. Panchal, Z. Zhu, Nanoarchitectonics of polymeric crown-ether analog of Tröger base combined with potassium iodide and acids synergy in fixation of CO_2 and epoxides, Mol. Catal. 545 (2023), 113241.
[64] M. Zhou, J. Chen, Z. Qu, Y. Du, J. Zhang, H. Jiang, R. Chen, Dimension and shape controllable ZIFs for highly-efficient chemical fixation of CO_2 without solvent and co-catalyst, Sep. Purif. Technol. 320 (2023), 124120.
[65] Q. Yi, T. Liu, X. Wang, Y. Shan, X. Li, M. Ding, L. Shi, H. Zeng, Y. Wu, One-step multiple-site integration strategy for CO_2 capture and conversion into cyclic carbonates under atmospheric and cocatalyst/metal/solvent-free conditions, Appl. Catal. B Environ. 283 (2021), 119620.
[66] H. Mao, M. Guo, H. Fu, K. Yin, M. Jin, C. Wang, Y. Zhao, Z. Dong, J. Liu, A Biomass-Ligand-Based Ru(III) complex as a catalyst for cycloaddition of CO_2 and epoxides to cyclic carbonates and a study of the mechanism, Eur. J. Inorg. Chem. 26 (2022), e202200624.
[67] Z. Fang, Z. Deng, X. Wan, Z. Li, X. Ma, S. Hussain, Z. Ye, X. Peng, Keggin-type polyoxometalates molecularly loaded in Zr-ferrocene metal organic framework nanosheets for solar-driven CO_2 cycloaddition, Appl. Catal. B Environ. 296 (2021), 120329.
[68] X. Fang, C. Liu, L. Yang, T. Yu, D. Zhai, W. Zhao, W.Q. Deng, Bifunctional poly (ionic liquid) catalyst with dual-active-center for CO_2 conversion: Synergistic effect of triazine and imidazolium motifs, J. CO_2 Util. 54 (2021), 101778.
[69] M. Qiu, J. Li, H. Wu, Y. Huang, H. Guo, D. Gao, L. Shi, Q. Yi, One-pot non-covalent heterogenization and aromatization of poly(ionic liquids) for metal-/cocatalyst-free and atmospheric CO_2 conversion, Appl. Catal. B Environ. 322 (2023), 122125.
[70] X. Liu, C. Hu, J. Wu, P. Cui, F. Wei, Defective NH_2-UiO-66 (Zr) effectively converting CO_2 into cyclic carbonate under ambient pressure, solvent-free and co-catalyst-free conditions, Chin. J. Chem. Eng. 43 (2022) 222–229.
[71] Q. Li, W. Dai, J. Mao, X. He, Y. Liu, Y. Xu, L. Yang, J. Zou, X. Luo, Facile integration of hydroxyl ionic liquid into Cr-MIL-101 as multifunctional heterogeneous catalyst for promoting the efficiency of CO_2 conversion, Micro Mesopor. Mater. 350 (2023), 112461.
[72] S. Yue, H.L. Qu, X.X. Song, X.N. Feng, Novel hydroxyl-functionalized ionic liquids as efficient catalysts for the conversion of CO_2 into cyclic carbonates undermetal/halogen/cocatalyst/solvent-free conditions, N. J. Chem. 46 (2022) 5881–5888.
[73] R. Yan, K. Chen, Z. Li, Y. Qu, L. Gao, H. Tong, Y. Li, J. Li, Y. Hu, K. Guo, Fixation of CO_2 into cyclic carbonates by halogen-bonding catalysis, ChemSusChem 14 (2021) 738–744.